JOURNAL OF MATERIALS SCIENCE 21 (1986) 2409–2417

Theory of electrical resistivity of metal-matrix composites at cryogenic and higher temperatures

FRANCESC S. ROIG
College of Creative Studies, Department of Physics, University of California 93106, USA
California 93106, USA

JACQUES E. SCHOUTENS*
MMCIAC, Kaman Tempo, 816 State Street, Santa Barbara, California 93102, USA

This paper presents a theory describing the electrical resistivity (conductivity) in the axial direction of unidirectional fibre-reinforced metal-matrix composite (MMC) materials at cryogenic and higher temperatures. The theory is derived from the solution of Boltzmann's equation. A triple-integral expression is obtained to describe the change in the electrical conductivity in the matrix metal due to electron scattering from the fibre surfaces. It is shown that at cryogenic temperatures, the electrical resistivity can rise by a factor of 2200 over a decrease in temperature of about 6 K below about 10 K. This effect is due entirely to electron scattering from fibre surfaces. The model developed shows that the composite resistivity agrees well with known experimental data at temperatures above 80 K. At very low temperatures, $\varrho_c(T)/\varrho_c(T_R) \sim (1 - CT^{-4})^{-1}$, where T is the absolute temperature. Shortcomings and implications of the theory are discussed.

1. Introduction

No theoretical analyses have been found which correctly predict the electrical resistivity (conductivity) of continuous fibre-reinforced metal-matrix composites (MMC) at cryogenic and higher temperatures. As the temperature decreases from room temperature the composite resistivity is expected to decrease steadily, until at cryogenic temperature, it will rise sharply by orders of magnitude. The steady decrease is due to thermal effects in the matrix which can be modelled as $\varrho(T) \sim T^n$, where $\varrho(T)$ is the temperature-dependent resistivity of the matrix, T is the absolute temperature and n is an exponent between 1 and 2 [1]. The sharp increase in resistivity at cryogenic temperature has been referred to by Dingle [2] and others [3–5] as the *size effect*. In the analysis of MMC resistivity (conductivity), the resistivity of the fibres is generally considered to be orders of magnitude greater than that of the matrix material. Therefore, the electrical conductivity of MMC is generally dominated by the matrix conductivity.

Although there are a number of macroscopic conductivity models to predict the electrical conductivity of MMC, no microscopic models, particularly those dealing with the electron behaviour at very low temperatures, could be found [6]. In fact, it appears that there are no conductivity data at these low temperatures [6]. Macroscopic models are of two kinds: conduction along the fibre and conduction transverse to the fibre direction. The first kinds are based on some variation of the rule of mixtures, assuming the matrix conduction to be dominant. The transverse electrical conductivity models exhibit various degrees of complexity [7–10] including concepts of percolation [11–13]. Both kinds of model do not correctly predict electrical conductivity or resistivity of MMC at room temperature and below, and fail altogether below liquid-nitrogen temperature. One reason for this failure is that these models do not account for the electron transport process for temperature conditions in which the electron-scattering mean free path is of the order of or greater than the spacing between fibres. Electron scattering is produced by the fibre surfaces which, on a macroscopic scale, manifests itself as a greatly increased resistance to current flow. Thus, the fibres act as scattering boundaries, thereby modifying considerably the electrical conduction of the composite.

In this paper, a theory is developed to describe the electron scattering process from fibre surfaces using a classical theory based on the solution of Boltzmann's equation. In a certain sense, the theory presented is the inverse of the problem solved by Dingle [2] for very thin wires and films. The resulting triple definite integral is integrated numerically and the results are applied to continuous fibre-reinforced MMC to predict the electrical resistivity below room temperature. The present theory is applicable only to conduction along the fibre direction.

*To whom correspondence should be addressed.

0022–2461/86 $03.00 + .12

2. Theory

This theory considers a single fibre of a non-conducting material (graphite, oxides, nitrides, boron, or other) in a metallic matrix, with the fibre in the z direction. A small electric field E is applied in the z direction. Let $\bar{v}$ be the velocity of an electron at a point $\bar{r}$ in the metal, where $\bar{r}$ originates at the fibre axis. The linearized Boltzmann equation in Cartesian coordinates is then

$$v_x \frac{\partial F^1}{\partial x} + v_y \frac{\partial F^1}{\partial y} + \frac{F^1}{\tau_0} = \frac{eE}{m^*} \frac{\partial F^0}{\partial v_z} \quad (1)$$

which describes electron transport in the matrix. In Equation 1,

$$F^1(\bar{v}, \bar{r}) = F(\bar{v}, \bar{r}) - F^0(\bar{v}) \quad (2)$$

represents the deviation of the electron distribution function F from the equilibrium distribution F^0. In Equation 1, m^* is the electron effective mass which is assumed to be a scalar quantity, and e is the electronic charge. The quantity τ_0 is the electron relaxation time between collisions in the bulk metal. The general solution of Equation 1 is [2]

$$F^1(\bar{v}, \bar{r}) = F_m^1(\bar{v}) \left[1 + G(\bar{v}) \exp\left(\frac{-|\bar{r} - \bar{r}_B|}{\tau_0 v} \right) \right] \quad (3)$$

where

$$F_m^1(\bar{v}) = \frac{e\tau_0 E}{m^*} \frac{\partial F^0}{\partial v_z} \quad (4)$$

is the solution in the bulk metal and

$$\frac{|\bar{r} - \bar{r}_B|}{\tau_0 v} = \frac{[(x - x_B)^2 + (y - y_B^2)]^{1/2}}{\tau_0 (v_x^2 + v_y^2)^{1/2}} \quad (5)$$

The point defined by $\bar{r}_B$ is on the fibre boundary or surface which is reached by proceeding backward from $\bar{r}$ along the direction of $\bar{v}$. The function $G(\bar{v})$ will be determined by the boundary condition on the surface of the fibre.

If

$$F^1 = F_m^1 + \Delta F^1 \quad (6)$$

with

$$\Delta F^1 = F_m^1(\bar{v}) G(\bar{v}) \exp\left(\frac{-|\bar{r} - \bar{r}_B|}{\tau_0 v} \right) \quad (7)$$

then the change in F_m^1 is due to scattering at the fibre surface. Thus, ΔF^1 experiences an exponential decrease as the point $\bar{r}$ of interest is moved away from the fibre boundary. The distance moved away from the fibre surface is called the *characteristic length* Λ_0, or the mean free path due to scattering.

If the cell region in the matrix is that region Λ_0 away from the fibre surface, then ΔF^1 is mainly determined by the scattering at the fibre boundary. The change in the current density Δj_c in this region is given [3] by the formula

$$\Delta j_c(x, y) \simeq -2e \left(\frac{m}{h} \right)^3 \iiint v_z \Delta F^1 \, dv_x \, dv_y \, dv_z \quad (8)$$

and the changes in the bulk conductivity of a region

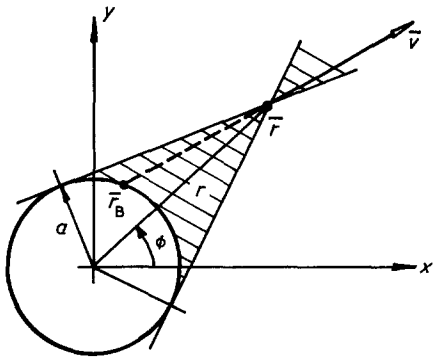

Figure 1 Coordinates of a point near a fibre surface used in the derivation of the theory.

due to fibre-boundary scattering is given by

$$\Delta\sigma_c = \frac{1}{EA_c} \iint_{\text{region}} \Delta j_c(x, y) \, dx \, dy \quad (9)$$

where A_c is the cross-sectional area of the region of interest.

Now, let Δj_c be the contribution due to the scattering at the fibre. This contribution is obtained by integrating ΔF_m^1 over all velocities whose directions are within the solid angle determined by the two tangent lines from $\bar{r}$ to the fibre surface, as shown in Fig. 1. For adjacent fibres of a real composite, scattering contributions from fibre surfaces whose distances to the point of interest in the integration are greater than Λ_0 are neglected. Equation 9 therefore can be written as

$$\Delta\sigma_c = \frac{1}{EA_c} \int_a^{a+\Lambda_0} r \, dr \int_0^{2\pi} \Delta j_c \, d\phi \quad (10)$$

where a is the fibre radius and r and ϕ are polar coordinates of the integration point (Fig. 1). Consequently, $\Delta\sigma_c$ is given by the change, due to one fibre, in the annular region $a \leqslant r \leqslant (\Lambda_0 + a)$ around the fibre, as shown in Fig. 2. Thus, this is the problem of scattering from the external surface of a cylinder and is the inverse of the problem solved by Dingle [2] wherein scattering occurred inside a cylinder of radius a.

If σ_0 is the conductivity of the bulk metal and j_0 is

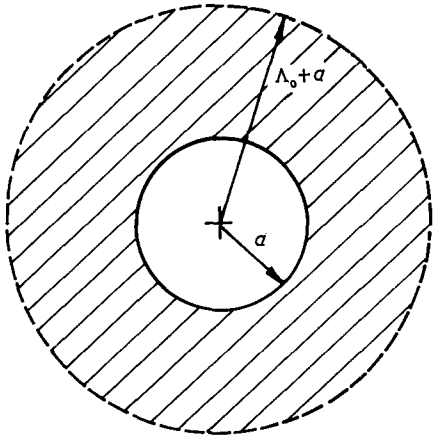

Figure 2 The shaded region shows the electron scattering region around a fibre.

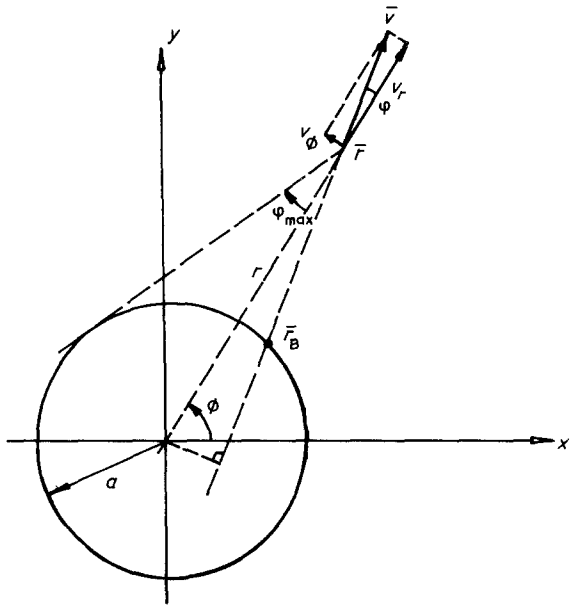

Figure 3 Coordinates and velocity components of $\bar{v}$.

the corresponding current density, then

$$\frac{\sigma}{\sigma_0} = \frac{\iint_{\text{region}} j_c(\bar{r})\,\mathrm{d}s}{\iint_{\text{region}} j_0\,\mathrm{d}s} \tag{11}$$

Letting $j_c(\bar{r}) = j_0 + \Delta j_c$, and since j_0 is independent of $\bar{r}$, Equation 11 can be written as

$$\frac{\sigma}{\sigma_0} = 1 + \frac{1}{A_c}\iint_{\text{region}} \frac{\Delta j_c(\bar{r})\,\mathrm{d}s}{j_0} \tag{12}$$

But

$$\iint \Delta j_c(\bar{r})\,\mathrm{d}s \tag{13}$$

is given by Equation 10 so that using cylindrical symmetry, Equation 12 becomes

$$\frac{\sigma}{\sigma_0} = 1 + \frac{2\pi}{A_c}\int_a^{a+\Lambda_0} \frac{\Delta j_c(r)}{j_0}\, r\,\mathrm{d}r \tag{14}$$

2.1. Solution of the Boltzmann equation

It is assumed that the distance separating fibres is greater than the electron-scattering mean free path. This means that scattering contributions within the region $a \leqslant r \leqslant (\Lambda_0 + a)$ are not negligible. When the fibre separation distance is of order Λ_0, contributions from other fibre surfaces at the point $\bar{r}$ of interest will occur, thus representing overlaps in scattering regions. At present, this case has not been calculated.

Now, following Dingle [2], cylindrical coordinates r and ϕ as shown in Fig. 3, are introduced: $x = r\cos\phi$, $y = r\sin\phi$, $z = z$, and for the velocity components

$$\begin{aligned} v_x &= v_r\cos\phi - v_\phi\sin\phi \\ v_y &= v_r\sin\phi + v_\phi\cos\phi \\ v_z &= v_z \end{aligned} \tag{15}$$

Using these coordinates and the fact that the problem has cylindrical symmetry, the Boltzmann Equation 1 becomes [2]

$$v_r\frac{\partial F^1}{\partial r} + \frac{v_\phi^2}{r}\frac{\partial F^1}{\partial v_r} - \frac{v_\phi v_r}{r}\frac{\partial F^1}{\partial v_\phi} + \frac{F^1}{\tau_0} = \frac{eE}{m^*}\frac{\partial F^0}{\partial v_z} \tag{16}$$

which has the general solution [2]

$$F^1 = \frac{eE\tau_0}{m^*}\frac{\partial F^0}{\partial v_z}\left[1 - f(rv_\phi, v_r^2 + v_\phi^2) \times \exp\left(-\frac{1}{\tau_0}\frac{rv_r}{v_r^2 + v_\phi^2}\right)\right] \tag{17}$$

where $f(\alpha, \beta)$ is an arbitrary function that must be even in the variable $\alpha = rv_\phi$, since F^1 has to be an even function of v_ϕ from symmetry of the problem. The boundary condition at the fibre surface determines the function $f(\alpha, \beta)$. This function is written as f_+ for $v_r > 0$ (electron motion away from the fibre) and f_- for $v_r < 0$ (electron motion toward the fibre). If p is the probability for an elastic scattering at the fibre surface, then the boundary condition at $r = a$ is

$$F(v_r, v_\phi; r = a) = pF(-v_r, v_\phi; r = a) + g \tag{18}$$

where $v_r > 0$, and g is the distribution function for diffusively or inelastically scattered electrons. Since $F = F^0 + F^1$, this function is

$$g = (1 - p)F^0 + F^1(v_r, v_\phi; r = a) - pF^1(-v_r, v_\phi; r = a) \tag{19}$$

where, using Equation 17,

$$F^1(v_r, v_\phi; r = a) = F_m^1(\bar{v}) \times \left[1 - p - f_+(av_\phi, v_r^2 + v_\phi^2) \times \exp\left(-\frac{av_r}{\tau_0(v_r^2 + v_\phi^2)}\right)\right] \tag{20}$$

and likewise

$$F^1(-v_r, v_\phi; r = a) = F_m^1(\bar{v}) \times \left[1 - p - f_-(av_\phi, v_r^2 + v_\phi^2) \times \exp\left(\frac{av_r}{\tau_0(v_r^2 + v_\phi^2)}\right)\right] \tag{21}$$

and finally

$$g = (1 - p)F^0 + F_m^1(\bar{v}) \times \left[1 - p - f_+(av_\phi, v_r^2 + v_\phi^2) \times \exp\left(-\frac{av_r}{\tau_0(v_r^2 + v_\phi^2)}\right) + pf_-(av_\phi, v_r^2 + v_\phi^2)\exp\left(\frac{av_r}{\tau_0(v_r^2 + v_\phi^2)}\right)\right] \tag{22}$$

The function g must be independent of direction, and since $F_m^1(\bar{v})$ depends on direction, it follows that

$$1 - p - f_+(av_\phi, v_r^2 + v_\phi^2)\exp\left(-\frac{av_r}{\tau_0(v_r^2 + v_\phi^2)}\right) + pf_-(av_\phi, v_r^2 + v_\phi^2)\exp\left(\frac{av_r}{\tau_0(v_r^2 + v_\phi^2)}\right) = 0 \tag{23}$$

As shown in Fig. 3, scattering from the fibre occurs only where $v_r > 0$ and for the condition

$$0 < \frac{v_r}{(v_r^2 + v_\phi^2)^{1/2}} < \sin \varphi_{max} \quad (24)$$

where $\sin \varphi_{max} = a/r$; otherwise, $f_+ = 0$ or $F^1 = F_m^1$. This occurs because there are no electrons scattered from any surface other than the fibre in the centre of the region of interest. Similarly, for $v_r < 0$, $F^1 = F_m^1$ and, therefore, $f_- = 0$. These results are confirmed by the form of the general solution (Equation 3).

Now, Equation 23 with $f_- = 0$ gives

$$f_+(av_\phi, v_r^2 + v_\phi^2) = (1 - p) \exp\left(\frac{av_r}{\tau_0(v_r^2 + v_\phi^2)}\right) \quad (25)$$

so that

$$f_+(rv_\phi, v_r^2 + v_\phi^2) = (1 - p) \times \exp\left(\frac{[a^2(v_r^2 + v_\phi^2) - r^2 v_\phi^2]^{1/2}}{\tau_0(v_r^2 + v_\phi^2)}\right) \quad (26)$$

and, therefore, the solution to the Boltzmann Equation 16 becomes

$$F^1 = F_m^1(\bar{v})\left[1 - (1 - p) \times \exp\left(-\frac{1}{\tau_0}\frac{rv_r - [a^2(v_r^2 + v_\phi^2) - r^2 v_\phi^2]^{1/2}}{(v_r^2 + v_\phi^2)}\right)\right] \quad (27)$$

when v_r and v_ϕ satisfy the condition of Equation 24, and $F^1 = F_m^1(\bar{v})$ otherwise.

2.2. Calculation of the conductivity

The conductivity is given by Equation 14. To calculate Δj_c, Equation 8 where the integral is performed in spherical coordinates (v, θ, φ) is used, with

$$\begin{aligned} v_r &= v \sin\theta \cos\varphi \\ v_\phi &= v \cos\theta \sin\varphi \\ v_z &= v \cos\theta \end{aligned} \quad (28)$$

Then, the solution of Equation 27 becomes

$$F^1 = \frac{e\tau_0 E}{m^*}\frac{\partial F^0}{\partial v_z}\left[1 - (1 - p) \times \exp\left(-\frac{[r\cos\varphi - (a^2 - r^2\sin^2\varphi)^{1/2}]}{\tau_0 \sin\theta}\right)\right] \quad (29)$$

and

$$\Delta j_c(r) = -2e\left(\frac{m}{h}\right)^3 \int_0^\infty v^2\,dv \times \int_0^\pi \sin\theta\,d\theta \int_{-\varphi_{max}}^{\varphi_{max}} \Delta F^1 v_z\,d\varphi \quad (30)$$

where, as shown in Fig. 3, $\varphi_{max} = \sin^{-1}(a/r)$. The current density due to the background scattering is

$$j_0 = -2e\left(\frac{m}{h}\right)^3 \int_0^\infty v^2\,dv \int_0^\pi \sin\theta\,d\theta \int_0^{2\pi} v_z F_m^1\,d\varphi \quad (31)$$

Then, as outlined elsewhere [2, 3],

$$\frac{\Delta j_c(r)}{j_0} = -(1 - p)\frac{3}{\pi}\int_0^{\pi/2}\cos^2\theta \sin\theta\,d\theta \int_0^{\varphi_{max}} \times \exp\left(-\frac{[r\cos\varphi - (a^2 - r^2\sin^2\varphi)^{1/2}]}{\Lambda_0 \sin\theta}\right)d\varphi \quad (32)$$

and substituting into Equation 14 gives for the conductivity ratio

$$\frac{\sigma}{\sigma_0} = 1 - (1 - p)\frac{6}{A_c}\int_a^{a+\Lambda_0} r\,dr \int_0^{\pi/2}\cos^2\theta \sin\theta\,d\theta \times \int_0^{\varphi_{max}} \exp\left(-\frac{[r\cos\varphi - (a^2 - r^2\sin^2\varphi)^{1/2}]}{\Lambda_0 \sin\theta}\right)d\varphi \quad (33)$$

For convenience of numerical integration, Equation 33 can be transformed to dimensionless variables by setting $x = r/a$ and $k = 2a/\Lambda_0$. Then, Equation 33 becomes

$$\frac{\sigma}{\sigma_0} = 1 - (1 - p)\frac{6a^2}{A_c} \times \int_1^{1+2/k} x\,dx \int_0^{\pi/2}\cos^2\theta \sin\theta\,d\theta \int_0^{\sin^{-1}(1/x)} \times \exp\left(-\frac{k[x\cos\varphi - (1 - x^2\sin^2\varphi)^{1/2}]}{2\sin\theta}\right)d\varphi \quad (34)$$

Equation 34 is the electrical conductivity of the matrix due to electron scattering from the fibre surface within a region Λ_0. It can be seen that this integral depends on the range x and, thus, affects the limit $\sin^{-1}(1/x)$ of the integral over φ. An analytical solution to Equation 34 has not been found.

3. Numerical integration

For numerical integration, Equation 34 can be written in the form

$$\frac{\sigma}{\sigma_0} = 1 - (1 - p)\frac{2\pi a^2}{A_c}\int_1^{1+2/k} x\,dx \times \left(\frac{3}{\pi}\int_0^{\pi/2} f(\theta)\,d\theta \int_0^{\varphi_{max}} h(x, \theta, \varphi)\,d\varphi\right) \quad (35)$$

where

$$f(\theta) = \cos^2\theta \sin\theta \quad (36)$$

$$h(x, \theta, \varphi) = \exp\left(-\frac{k}{2\sin\theta}[x\cos\varphi - (1 - x^2\sin^2\varphi)^{1/2}]\right) \quad (37)$$

The following nested Simpson's rule integration was used to calculate Equations 35, 36, and 37. Defining the integral by $I(k)$,

$$I(k) = \frac{\Delta_0}{3}(x_0 C_0 + 4x_1 C_1 + 2x_2 C_2 + \ldots + 4x_{n-1} C_{n-1} + x_n C_n) \quad (38)$$

where Δ_0, Δ_1 or Δ_2 is the integration step,

$$C_i = \frac{3}{\pi}\left[\frac{\Delta_1}{3}(f_0D_0 + 4f_1D_1 + 2f_2D_2 + \ldots + 4f_{n-1}D_{n-1} + f_nD_n)\right] \quad (39)$$

and

$$D_j = \frac{\Delta_2}{3}(h_0 + 4h_1 + 2h_2 + \ldots + 4h_{n-1} + h_n) \quad (40)$$

Equation 40 is therefore an integral of $h(x, \theta, \varphi) = h(x_i, \theta_j, \varphi) \equiv A_j$ over all values of φ at a given value of x_i and θ_j. Likewise, Equation 39 is an integral of $f(\theta)$ for all θ and a fixed x_i. Thus, more explicitly, any term in Equation 38 is

$$mx_iC_i = mx_i\left\{\frac{\Delta_1}{3}\left[f_0\left(\frac{\Delta_2}{3}(h_0 + 4h_1 + \ldots + h_n)\right) + 4f_1\left(\frac{\Delta_2}{3}(h_0 + 4h_1 + \ldots + h_n)\right) + \ldots + f_n\left(\frac{\Delta_2}{3}(h_0 + \ldots + h_n)\right)\right]\right\} \quad (41)$$

where m is either 4 or 2, and for $i = 0$ or $i = n$, $m = 1$. Thus, D_j is a single integral, C_i is a double integral, and $I(k)$ is the triple integral given by Equation 35.

The calculations were performed on Hewlett-Packard HP-41C hand-held calculator with three memory modules and a magnetic card reader adapter to record the program instructions. The program logic was checked out by using $f(\theta) = \cos\theta$ and $h(x, \theta, \varphi) = kx \sin\theta \cos\varphi$ so that the ingration logic of the first two integrals can be checked, and also to test the conversion dependence on the number of integrating steps. These functions were chosen so that the integral of Equation 35 could be done analytically as a check on the logic. The logic of the integral over x was checked by setting the integrals over θ and φ equal to unity at each step. The integration was carried out for eleven values of k between 0.5 and 2.0 and was found to represent a straight line in a plot of ln N against ln k. $I(k)$ is shown in Fig. 4. Each point required 35 min of computation time on the HP-41C and conversion was easily obtained in six steps ($n = 6$).

Initially, an attempt was made to simplify the numerical computation by writing Equation 35 as

$$\frac{\sigma}{\sigma_0} = 1 - (1 - p)\frac{2\pi a^2}{A_c}\int_1^{1+2/k} f(x)x\,dx \quad (42)$$

where $f(x)$ is a curve fit to the integrals over θ and φ. An excellent curve fit could be obtained with $f(x) = Cx^{-n}$, where C is a constant. However, when integrated for each value of k, n increased with increasing values of k from 1.1 to 12.8. One value was close to $n = 2$, causing a singularity in the integral in Equation 42. Another function of form $f(x) = C\,e^{-\alpha x}$ was attempted. When integrated, this function gave a sigmoidal-shaped curve departing considerably from

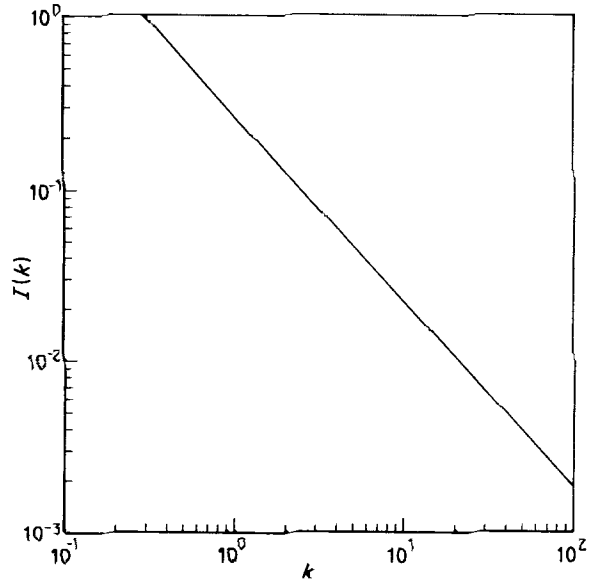

Figure 4 Values of the integral $I(k)$ as a function of k where $k = 2a/\Lambda_0$. Integration step: $n = 6$.

that of Fig. 4. Moreover, as $k \to 0$, the integral in Equation 42 approached a constant. Therefore, although this kind of simplification at first appeared to simplify numerical integration, it turned out to be unworkable. It has not been possible to check $I(k)$ against its "real" value because a way to perform the integrals analytically has not been found. It is expected that the numerical integration error is of order $\Delta^4(x_n - x_0)f^{iv}(\delta)/180$ for each integral, where $x_0 < \delta < x_n$ [14], but this has not been studied. Here, $f^{iv}(\delta)$ is the fourth derivative of the function evaluated at δ [14].

4. Derivation of the composite conduction

Equation 34 can be written to show temperature dependence for a composite or

$$\frac{\sigma_c(T)}{\sigma_c(T_R)} = 1 - (1 - p)\frac{2\pi a^2}{A_c}I(k) \quad (43)$$

where $\sigma_c(T)$ and $\sigma_c(T_R) \simeq \sigma_0(1 - V_f)$ are the composite temperature at any temperature and room temperature, respectively, and $I(k)$ is the numerical value of the triple integral for a given value of k. The parameter p is the scattering probability for electrons from the fibre surfaces, which can also be viewed as a fibre-surface characteristic or, to use Ziman's expression [15], the surface polish. Microstructural examination of the fibre shows its surface to be fairly irregular compared to the lattice dimensions, so that electrons are scattered diffusively. Hence, it is considered that $p \equiv 0$ in Equation 43. For a perfectly polished surface, $p = 1$, implying that $\sigma_c(T)/\sigma_c(T_R) = 1$. This means that the electrons do not scatter and there is no change in the matrix conductivity except from thermal scattering.

As Λ_0 increases (k decreases since $k = 2a/\Lambda_0$, where a is the fibre radius), $\sigma_c(T)/\sigma_c(T_R) \to 0$, implying that the matrix resistivity increases without any bound (theoretically speaking) due to scattering from the fibres. This boundary scattering has been discussed extensively elsewhere [2–5, 15–17]. The scattering

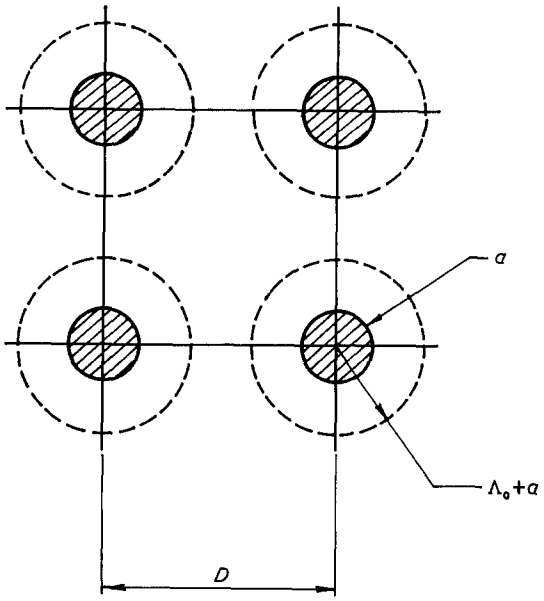

Figure 5 Composite cell used in deriving a conductivity model for MMC.

mean free path Λ_0 is inversely dependent upon temperature so that $I(k) \sim T^n$, where n is a constant. Below, a relationship between k and T is derived so that the results of Equation 43 can be related to the material temperature.

4.1. Derivation of conduction equation

Fig. 5 shows an idealized composite cell of average size D with fibres at each corner, with their axes normal to the plane of the paper and the radius a. The dashed concentric circles indicate the regions with radius $(\Lambda_0 + a)$, centred on the fibres, of the mean free path of electrons scattered from the fibre surfaces. In this model, it is assumed that $a \leqslant (\Lambda_0 + a) \lesssim D$, and the overlap of scattering is not considered. (Consideration of the overlap of scattering regions requires a more complex analysis that takes into account the p values of each fibre as well as the scattering contribution from all surrounding fibres, possibly with a coordination number of 12.) For the case of no overlap in scattering regions, the conductivity within the cell in Fig. 5 consists of two additive parts: that contributed by the composite at room temperature and that contributed by the scattering region. Therefore, the composite conductivity at T is

$$\sigma_c(T) = \sigma_c(T_R) + \sigma_{sc}(T) \quad (44)$$

In Equation 44, $\sigma_c(T_R) \simeq \sigma_0(1 - V_f)$, where σ_0 is the bulk conductivity, where fibre conductivity is neglected since $\sigma_f \ll \sigma_0$. As the temperature of the composite is reduced, the scattering region grows, decreasing the composite conductivity by an amount equal to the scattering contribution times the ratio of the areas of scattering and the cell. Thus

$$\sigma_{sc}(T) = -(1 - p)\frac{2\pi a^2}{A_c} I(k) \frac{A_{sc}}{A_c} \sigma_c(T_R) \quad (45)$$

Substituting Equation 45 into Equation 44 gives

$$\frac{\sigma_c(T)}{\sigma_c(T_R)} = 1 - (1 - p)\frac{2\pi a^2}{A_c} I(k) \frac{A_{sc}}{A_c} \quad (46)$$

The total volume of the cell per unit axial length is $v_T = D^2$, and the total volume of fibre per unit axial length is $v_f = \pi a^2$, so that the fibre volume fraction of the cell is

$$V_f = \pi\left(\frac{a}{D}\right)^2 \quad (47)$$

The cross-sectional area A_c of the cell is $A_c = D^2 - \pi a^2$ or, using Equation 47,

$$A_c = D^2(1 - V_f) \quad (48)$$

Now, the area of the scattering region is $A_{sc} = \pi[\Lambda_0^2 + 2a\Lambda_0]$ which, when using the relation between k and Λ_0, gives

$$A_{sc} = 4\pi a^2 \frac{1 + k}{k^2} \quad (49)$$

Substituting Equations 48 and 49 into Equation 45 gives

$$\frac{\sigma_c(T)}{\sigma_c(T_R)} = 1 - (1 - p)\left(\frac{V_f}{1 - V_f}\right)^2 \frac{8(1 + k)}{k^2} I(k) \quad (50)$$

As argued above, for real composites, $p \equiv 0$. Moreover, since composite resistivity is of interest for comparison with experimental data, Equation 50 must be inverted. This yields the resistivity as

$$\frac{\varrho_c(T)}{\varrho_c(T_R)} = \left[1 - \left(\frac{V_f}{1 - V_f}\right)^2 \frac{8(1 + k)}{k^2} I(k)\right]^{-1} \quad (51)$$

Note that as $k \to \infty$ $(\Lambda_0 \to 0)$, the second term in the bracket vanishes and $\varrho_c(T)/\varrho_c(T_R) \to 1$, as it should at room temperature. This is in agreement with the experimental data of Abukay *et al.* [1] for Al–60 vol % B composite. Their measured value of resistivity at room temperature is essentially that given by the usual model $\varrho_c/\varrho_0 = (1 - V_f)^{-1}$ (see Equation 3 in Abukay *et al.* [1]) for resistivity in the fibre direction. Conversely, as $k \to 0$, $\varrho_c(T)/\varrho_c(T_R) \to \infty$ (in theory). In practice, this is not the case since the mean free path approaches a limit as the temperature approaches absolute zero because of the lattice dislocations, impurities, and other effects [15–17].

Now it is necessary to relate k with temperature. No simple model has been found that relates the mean free path in an alloy to temperature. Such calculations are extremely complex [15, 18] and have not been attempted here. However, a simple useful relation can be derived that can also be "calibrated" to composites. First, note that $I(k)$ is a linear function in k, so that a simple regression analysis for a sufficiently large sample of values (25 in this instance) gives

$$I(k) = 0.27k^{-1.08} \quad (52)$$

with the coefficient of determination of $r^2 = 1.00$.

A linear relationship between k and T can also be written, assuming such a relationship exists, or

$$T = Ck \quad (53)$$

where C is a constant. To determine the value of this constant, the following argument is used. At room

TABLE I Values of lowest temperature T_l for the present model

V_f	T_l (K)
0.10	1.30
0.20	2.02
0.30	2.68
0.40	3.33
0.50	3.98
0.60	4.66
0.70	5.36
0.80	6.11
0.90	6.91

temperature Λ_0 is close to zero, making k large. Using Equations 51 and 52 shows that $\varrho_c(T)/\varrho_c(T_R) = 1$ within 2 parts in 10^5 when $k = 100$. Considering $T_R = 300\,K$, Equation 53 gives $C = 3$.

In this model, the effect of overlapping electron scattering regions is neglected and it is assumed that $\Lambda_0 + a = D$ in the limit. This sets a lower bound on k. Substituting $k = 2a/\Lambda_0$ and using Equation 47, the lower bound on k becomes

$$k_l = \frac{2(V_f/\pi)^{1/2}}{1 - (V_f/\pi)^{1/2}} \quad (54)$$

Using Equations 53 and 54 to find the lowest temperature for this model yields

$$T_l = \frac{6(V_f/\pi)^{1/2}}{1 - (V_f/\pi)^{1/2}} \quad (55)$$

Values of T_l against V_f are given in Table I. The meaning Equation 55 is that temperatures less than T_l have no physical meaning in this model because then $\varrho_c(T)/\varrho_c(T_R) < 0$. The implication of the above analysis is that if $I(k)$ is linearly related to k and a linear relationship between k and T is assumed, then

$$I(k) = 0.88T^{-1.08} \quad (56)$$

which results from combining Equations 52 and 53. Substituting Equation 56 into Equation 51 gives

$$\frac{\varrho_c(T)}{\varrho_c(T_R)} = \left[1 - 21.23\left(\frac{V_f}{1 - V_f}\right)^2 (3 + T)T^{-3.08}\right]^{-1} \quad (57)$$

TABLE II Resistivity ratio for $V_f = 0.25$ as function of absolute temperature

T (K)	$\varrho_c(T)/\varrho_c(T_R)$
2.2665	1633.8
2.2670	835.9
2.2675	561.9
2.2680	423.2
2.269	283.2
2.270	213.2
2.280	61.7
2.29	36.3
2.30	25.8
2.50	4.38
3.00	1.92
5.00	1.15
10.00	1.026
20.00	1.0054
30.00	1.0022
50.00	1.0007
100.00	1.0002

TABLE III Resistivity ratio for $V_f = 0.35$ as function of absolute temperature

T (K)	$\varrho_c(T)/\varrho_c(T_R)$
3.2755	2948.5
3.2760	1371.0
3.2765	893.3
3.2770	622.6
3.2775	526.6
3.2780	437.0
3.2785	373.5
3.2900	86.4
3.30	52.1
3.40	10.96
3.60	4.67
3.80	3.18
4.00	2.516
6.00	1.286
8.00	1.126
10.00	1.071
20.00	1.0141
30.00	1.0058
50.00	1.0019
100.00	1.0004

Results of calculations with Equation 57 beginning with the lowest temperatures up to 100 K are shown in Table II for $V_f = 0.25$, Table III for $V_f = 0.35$, and Table IV for $V_f = 0.50$. These values of V_f are representative of fibre volume fraction of MMC. For values of T less than the first indicated temperature in these tables, $\varrho_c(T)/\varrho_c(T_R) < 0$, which is physically meaningless. For values of T greater than the lowest value, $\varrho_c(T)/\varrho_c(T_R)$ decreases very sharply. This trend is in agreement with the results of theories developed by Dingle [2] and discussed elsewhere [15–17].

5. Discussion

The values listed in Tables II to IV show that (i) a very steep rise in composite resistivity occurs at temperatures below about 10 K, and (ii) at $T > 10\,K$, the composite resistivity is essentially the value at room temperature, in agreement with experimental data [1]. The steep rise in resistivity at very low temperature is due entirely to the effects of electrons scattered from the fibre surfaces. This resistivity can be orders of magnitude above the bulk values. On average, for

TABLE IV Resistivity ratio for $V_f = 0.50$ as function of absolute temperature

T (K)	$\varrho_c(T)/\varrho_c(T_R)$
5.3776	3038.6
5.3780	1959.4
5.3785	1357.1
5.3790	1038.1
5.3800	706.2
5.3850	272.1
5.390	168.7
5.395	122.4
5.400	96.09
5.50	18.64
6.00	4.282
8.00	1.629
10.00	1.2980
20.00	1.0505
30.00	1.0202
50.00	1.0066
100.00	1.0015

calculations presented in this paper, this rise amounts to a factor of about 2200 for a decrease of 6 K in temperature below 10 K. Equation 57 shows that

$$\frac{\varrho_c(T)}{\varrho_c(T_R)} \sim (1 - CT^{-4})^{-1} \quad (58)$$

for very low temperature, and that in the limit of room temperature, $\varrho_c(T)/\varrho_c(T_R) \to 1$, or $\varrho_c(T_R)/\varrho_0 \simeq (1 - V_f)^{-1}$, as it should be. This conclusion is in agreement with the findings of Abukay *et al.* [1].

The electrical conductivity of MMC depends also on the post-fabrication heat treatment, as discussed by Jenkins and Arajs [19]. They showed that matrix annealing temperatures ranging from 298 to 873 K will result in a general reduction in the composite resistivity of about a factor of two. These data are for Al–28 vol % graphite where the graphite fibre is Thornel 50.

Jenkins and Arajs [19] also showed that the decrease in resistivity with increasing annealing temperature for Al–28 vol % graphite is linear. However, this appears to be incorrect. Despite the large error bars in their data, the distribution in the datum points would indicate that this decrease follows the recovery and recrystallization profiles for heat-treated alloys [20].

Aside from resistivity decreases due to annealing, Jenkins and Arajs [19] also observed a linear decrease in resistivity with temperature of about a factor of 2.5 for the same composite within a temperature range decreasing from 290 to 80 K. This linear decrease is due to thermal effects in the alloy and has nothing to do with the electron scattering effects discussed in this paper. This linear decrease was also observed for Al–60 vol % B in the axial and transverse directions [1]. The linear decrease can be well represented by a functional relationship of the form

$$\varrho_0(T) = \varrho_0(T_R)\left(\frac{295}{T}\right)^C \quad (59)$$

where $\varrho_0(T_R)$ is the bulk resistivity at room temperature, T_R, taken as $3.3 \times 10^{-6}\,\Omega$cm [1], and the constant $C = -1.45$ for the same data [1]. Equation 59 is not valid when $T/\Theta \lesssim 0.2$, where Θ is the Debye temperature [18].

The adaptation of the theory discussed in this paper presents some difficulties, as discussed in the following.

Equation 43 depends on the cell cross-sectional area A_c, which is somewhat arbitrarily defined. The analysis is based on a square array to define A_c and A_{sc}, but the resulting Equation 57 does not depend on any specific geometry. The theory does not account for the overlapping electron scattering regions, the effects of which have not yet been calculated. In real composites, the arrays of fibres are arranged in a somewhat random fashion [21]. This gives rise to overlapping regions as shown in Fig. 6. As the size of reinforcing fibre increases, order appears out of randomness and the fibre distribution appears as quasi-square or hexagonal arrays [22]. This is due mostly to fabrication methods. For small-diameter closely-spaced fibres, many fibres are in physical contact. Consequently, the degree of overlap in the scattering regions

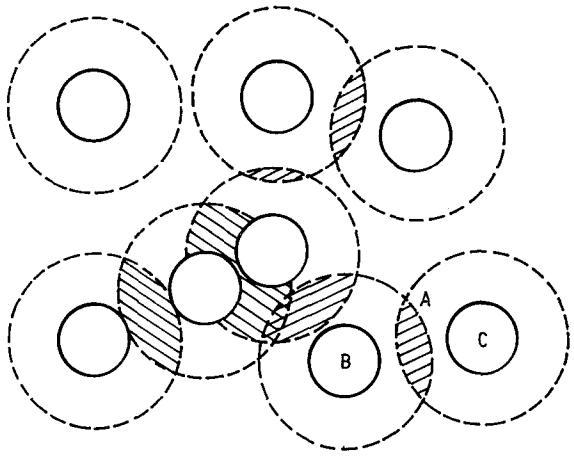

Figure 6 Appearance of real arrays of small fibres in a metal-matrix composite, showing equal scattering regions (fixed temperature) overlapping due to fibre distance smaller than Λ_0.

varies a great deal. These are shown as cross-hatching in Fig. 6. Within such regions (for example, Region A in Fig. 6), contributions to electron scattering come from Fibres B and C. Therefore, the integral in Equation 34 must be modified.

It is known from the theory of metals that electron transport is very sensitive to lattice defects and impurities. In a pure crystal, electron motion is unimpeded except by thermal effects at high temperatures. Thus, one would expect the mean free path in a pure crystal at low temperature to be very large, on the order of 10^3 to $10^5\,\mu$m [17]. The value of the resistivity in pure metals is generally proportional to the absolute temperature for $T \sim \Theta$, where Θ is the Debye temperature. When $T \ll \Theta$, the resistivity is $\varrho \sim T^5/M\Theta^6$, where M is the mass of the lattice atoms and for aluminium, $\Theta = 390$ K. On the other hand, the resistivity of a metal containing foreign atoms in solid solution is nearly always greater than that of the pure metal, and the increase is considerable in many cases. In general, this increase is independent of temperature (Matthiessen's rule) [18].

The greatest weakness of the theory presented is the connection made between the integral $I(k)$ and T through an assumed linearity between k and T. Thus, some arbitrariness exists in selecting the lowest temperature, in other words in "calibrating" the theory by means of a parameter in the absence of data. A physical approach is to relate Λ_0 to T from a detailed theory supported by experimental data. As far as is known, this has not been done for MMC at liquid-hydrogen or liquid-helium temperatures [6]. The mean free path Λ_0 is a function of lattic defects and impurities and alloy structure. Typical grain dimensions in aluminum alloys are on the order of 1 to 10 μm. Consequently, at cryogenic temperatures, one would expect the upper limit of the electron mean free path not to exceed 1 to 10 μm. Thus, for $\Lambda_0 \simeq 5\,\mu$m, $k \simeq 30/5 = 6$ when the fibre diameter is approximately 30 μm [21]. From Equation 53, then, $T \simeq 18$ K. According to the theory developed in this paper, at this temperature, $\varrho_c(T)/\varrho_c(T_R) \simeq 1.12$ to 1.065 for $V_f = 0.25$ to 0.50, respectively. However, these estimates are based upon the constant $C = 3$ in Equation 53, which is derived

from heuristic arguments. Therefore, T_l is not adequately defined. For obvious reasons, $T = 0$ cannot be used because then $\varrho_c(T)/\varrho_c(T_R) < 0$ in this model. The conclusion, then, is that, in the absence of adequate theory for Λ_0 as a function of T and the apparent lack of experimental data [6], the present theory can only predict the trend expected in the composite resistivity at cryogenic temperatures.

Acknowledgement

The authors gratefully acknowledge and wish to thank Mr Louis A. Gonzalez, Director, MMCIAC, for helpful discussions and his support.

References

1. D. ABUKAY, K. V. RAO, S. ARAJS and Y. D. YAO, *Fiber Sci. Tech.* **10** (1977) 313.
2. R. B. DINGLE, *Proc. R. Soc.* **201A** (1949) 545.
3. E. H. SONDHEIMER, *Phys. Rev.* **80** (1950) 401.
4. R. G. CHAMBERS, *Proc. R. Soc.* **202A** (1950) 378.
5. D. K. C. MacDONALD and K. SARGINSON, *ibid.* **203A** (1951) 223.
6. S. ARAJS, personal communication (1985).
7. W. K. LIEBMANN and E. A. MILLER, *J. Appl. Phys.* **34** (1963) 2653.
8. J. W. RAYLEIGH, *Phil. Mag.* **34** (1892) 481.
9. L. K. H. van BECK, "Progress in Dielectrics", Vol. 7 (Heywood, London, 1967) p. 69.
10. W. E. A. DAVIES, *J. Phys. D* **7** (1974) 120.
11. T. JOY and W. STRIEDER, *J. Phys. C* **11** (1978) L867.
12. *Idem, J. Comp. Mater.* **13** (1979) 102.
13. *Idem, J. Phys. C* **12** (1979) L279.
14. G. P. WEEG and G. B. REED, "Introduction to Numerical Analysis" (Blaisdell, Waltham. Massachusetts, 1966), Ch. 4.
15. J. M. ZIMAN, "Electrons and Phonons" (Oxford University Press, London, 1962) Ch. XI.
16. C. R. TELLIER and A. J. TOSSER, "Size Effects in Thin Films" (Elsevier, Amsterdam, 1982).
17. J. M. ZIMAN "Principles of the Theory of Solids" (Cambridge University Press, 1965) Ch. 7.
18. N. F. MOTT and H. JONES, "The Theory of the Properties of Metals and Alloys" (Dover, New York, 1958) p. 286.
19. T. A. JENKINS and S. ARAJS, *Fiber Sci. Tech.* **17** (1982) 205.
20. J. D. VERHOEVEN, "Fundamentals of Physical Metallurgy" (Wiley, New York, 1975), Fig. 10.5, p. 331.
21. E. G. KENDALL, in "Composite Materials", Vol. 4, edited by L. J. Broutman and R. H. Krock (Academic Press, New York, 1974) Fig. 38, p. 368.
22. K. G. KREIDER and K. M. PREWO, in "Composite Materials", Vol. 4, edited by L. J. Broutman and R. H. Krock (Academic Press, New York, 1974) Fig. 9, p. 421.

Received 4 June
and accepted 18 September 1985